Check for updates

Geophysical Research Letters

RESEARCH LETTER
10.1029/2021GL096292

Frictional Characteristics of Oceanic Transform Faults: Progressive Deformation and Alteration Controls Seismic Style

Sophie Cox[1], Matt J. Ikari[2], Christopher J. MacLeod[1], and Åke Fagereng[1]

[1]School of Earth and Environmental Sciences, Cardiff University, Cardiff, UK, [2]MARUM, Centre for Marine Environmental Sciences and Faculty of Geoscience, University of Bremen, Bremen, Germany

Key Points:

- Dolerite hydrothermally cemented at greenschist facies is strong and velocity-weakening at 10 MPa normal stress and room temperature
- Natural fault rocks comprising chlorite-rich, fractured, and comminuted metadolerite are frictionally weak and velocity-strengthening
- Along oceanic transform faults, in the mafic oceanic crust, increased damage and alteration can explain fault weakness and aseismic slip

Supporting Information:

Supporting Information may be found in the online version of this article.

Correspondence to:

S. Cox,
coxs8@cardiff.ac.uk

Citation:

Cox, S., Ikari, M. J., MacLeod, C. J., & Fagereng, Å. (2021). Frictional characteristics of oceanic transform faults: Progressive deformation and alteration controls seismic style. *Geophysical Research Letters*, *48*, e2021GL096292. https://doi.org/10.1029/2021GL096292

Received 23 SEP 2021
Accepted 6 DEC 2021

© 2021. The Authors.
This is an open access article under the terms of the Creative Commons Attribution License, which permits use, distribution and reproduction in any medium, provided the original work is properly cited.

Abstract Oceanic transform faults are inferred to be weak relative to surrounding oceanic crust and primarily slip aseismically. Neither their weakness nor tendency to creep are well-explained. We test the effects of fault-rock evolution on oceanic transform fault frictional strength and stability using direct-shear experiments (at room temperature, 10 MPa normal stress, and fluid-saturated conditions) on dolerite from the East Pacific Rise and natural fault rocks from the exhumed Southern Troodos Transform, Cyprus. Dolerites and cemented breccias are frictionally strong ($\mu = 0.52–0.85$) and velocity-weakening (strength decreases with increasing slip velocity, characteristic of earthquakes). In contrast, matrix-rich chlorite-bearing fault breccias and gouges are frictionally weak ($\mu = 0.25–0.48$) and velocity-strengthening (characteristic of stable creep). This transition implies that seismic behavior is controlled by degree of damage and alteration, such that earthquakes can nucleate within relatively intact oceanic crust, whereas fault segments of increased damage and chlorite content tend to slip aseismically.

Plain Language Summary Oceanic transform faults are plate boundary faults where motion of oceanic lithosphere is dominantly horizontal and parallel to tectonic motion. Fewer and smaller earthquakes than expected occur along these faults, which are also considered weak structures. The reasons for their weakness and lack of large earthquakes are puzzling. To understand these characteristics, we conducted laboratory deformation experiments using rocks collected from the ocean floor (near Hess Deep in the Pacific) and from an ancient transform fault (in Cyprus). We sheared cylindrical samples, holding one half in place and sliding the other over it, creating laboratory equivalents of geological faults. We find that dolerite, one of the primary rock-types of the oceanic crust, is strong and capable of starting earthquakes. In contrast, we find that already damaged and altered rocks, found within natural faults (containing an increased proportion of the mineral chlorite), are weak. The same damage and alteration responsible for the weakness also prevents earthquakes. Our findings suggest that variations in the size and number of earthquakes on oceanic transform faults is controlled most of all by how damaged the existing rock is and how much alteration to weak, water-bearing secondary minerals such as chlorite has occurred along fault planes.

1. Introduction

Oceanic transform faults have low seismic coupling, and display far fewer and smaller earthquakes than expected from fault length-magnitude scaling relations, based on the Harvard centroid moment tensor catalog (e.g., Bird et al., 2002). Instead, up to 95% of displacement occurs aseismically, despite the faults cross-cutting the brittle mafic crust (Boettcher & Jordan, 2004). This earthquake deficit has been explained in two ways: (a) oceanic transforms experience both earthquakes and aseismic creep along the same fault segments, but at different times (e.g., Abercrombie & Ekström, 2001; Hilley et al., 2020; McGuire et al., 1996); and/or (b) oceanic transforms are segmented into "locked patches" hosting quasi-periodic earthquakes of Mw > 6.0, and microseismically active "rupture barriers" dominated by creep (e.g., McGuire, 2008; McGuire et al., 2005, 2012; Sykes & Ekström, 2012; Wolfson-Schwehr et al., 2014). Several recent studies have linked seismic style to alteration and damage of rocks. Throughout the crust and upper mantle, variable fault zone damage inferred from geophysically constrained mechanical properties (e.g., Froment et al., 2014; Roland et al., 2012), coupled to enhanced fluid circulation and growth of frictionally weak, hydrous phyllosilicates (e.g., Roland et al., 2010), provides one hypothesis to explain persistent along-strike segmentation in seismic behavior. Models for the rheology of high-strain mylonites indicate that seawater infiltration may control rheology and modulate the proportions of seismic and aseismic slip at temperatures >300 °C (Kohli et al., 2021). This hypothesis has, however, not been tested against direct geological or mechanical observations on oceanic crustal rocks at $T < 300$ °C.

On geological time scales, the stress state of oceanic transforms requires them to be mechanically weak relative to the surrounding crust (Zoback, 1991). Many mechanisms have been proposed to explain the inherent weakness of oceanic transforms in the shallow, brittle regime, including hydration of mafic and ultramafic minerals to frictionally weak (friction coefficient, μ, <0.6) phyllosilicates and serpentine (Behn et al., 2007; Moore et al., 1997), and elevated fluid pressure lowering the effective normal stress (Bergerat et al., 2000; Sykes & Ekström, 2012). Interconnected phyllosilicates have also been inferred to promote aseismic (velocity-strengthening) behavior of weak, mature continental faults (e.g., Imber et al., 1997; Schleicher et al., 2012). Within the oceanic lithosphere, the specific phyllosilicate chlorite has been found to contribute to strain localization along weak oceanic detachment faults (Escartín et al., 2003; MacLeod et al., 2002). However, there is a lack of geological or laboratory deformation evidence for comparable processes occurring along oceanic transforms; instead, experimental data on basalt and gabbro deformation have shown velocity-weakening behavior and $\mu \geq 0.6$ (Cox, 1990; He et al., 2007; Phillips et al., 2020; Zhang et al., 2017). If, however, creeping segments host increased damage and alteration, there is a need for targeted experiments on damaged and/or altered oceanic rocks. Here, we present the results of the first laboratory direct-shear friction experiments targeting a natural sample set of dolerite and dolerite-derived fault rocks from an oceanic transform fault. The data test the hypothesis that progressive evolution in fault rock damage controls both oceanic transform fault strength and slip style.

2. Materials and Methods

2.1. Samples

We obtained frictional properties of two intact dolerite samples dredged from the fast-spreading East Pacific Rise (EPR) (RRS *James Cook* cruise JC21; MacLeod et al., 2008). We did likewise from natural fault rocks (named following Sibson, 1977) collected from the sheeted dolerite dyke layer within the exhumed Southern Troodos Transform Fault Zone (STTFZ), Cyprus, that represent minor (cemented breccia), moderate (matrix-rich breccia), and intense (fault gouge) deformation and alteration (Figures 1 and 2a). The proportion of relatively intact dolerite clasts within the fault rocks was used as a proxy for fault zone damage, with decreasing clast proportion representing increased alteration and strain. Clast proportions for the various fault rocks were obtained by manually outlining clasts in Adobe Illustrator and determining proportions using ImageJ (FIJI) version 2.0.0 from backscattered scanning electron images of the samples prior to experiments.

The relatively intact EPR dolerites experienced typical hydrothermal alteration at greenschist facies conditions and contain ~60% plagioclase, ~30% pyroxene/actinolite, and ~5–10% chlorite within the crystalline ophitic texture. One of the dolerite samples (fractured dolerite) also contains variably oriented fractures. Of the STTFZ material, the cemented dolerite breccia comprises ~75% dolerite clasts (~0.2–9.0 mm), that are also altered to albite, actinolite, and <10% chlorite, within a fine-grained matrix that contains the same minerals, in approximately the same proportions as the dolerite clasts, and no obvious fabric. The matrix-rich breccia sample contains ~45% dolerite clasts (~0.1–9.0 mm) surrounded by chlorite-rich matrix. Our fault gouge sample comprises a foliated chlorite-rich matrix with only ~25% dolerite clasts (~0.05–4.5 mm) and minor amounts of quartz and calcite, minerals that are absent from the other samples.

2.2. Experimental Methods

Friction experiments were carried out using a GIESA RS5 single direct-shear apparatus (Figure 2b) (following Ikari et al., 2015) at the Marum Research Faculty at the University of Bremen, Germany, at room temperature (~20 °C in a climate-controlled room), 10 MPa normal stress (σ_n), and under fluid-saturated conditions (3.5% NaCl brine), appropriate for samples deforming within the upper crust of a vertical oceanic transform, where brittle deformation is expected. For one sample (intact dolerite), the peak strength at 10 MPa σ_n exceeded the apparatus limit and it was therefore initially broken under 1 MPa σ_n, before increasing the load to 10 MPa for the velocity-step test.

All five samples were run both as minicores, with any *in situ* fabric parallel to the shearing plane of the experiment apparatus, and as powders (grain size <125 μm). To deform the cylindrical (~20 mm in height, 25 mm diameter) samples, the direct-shear apparatus induces a "localized" shear plane within the sample (Figure 2b). The direct-shear apparatus has two horizontal displacement sensors (Figure 2b), one which monitors the machine driving or load point velocity (V_{lp}) and one measuring the offset of the cell plates and the sample

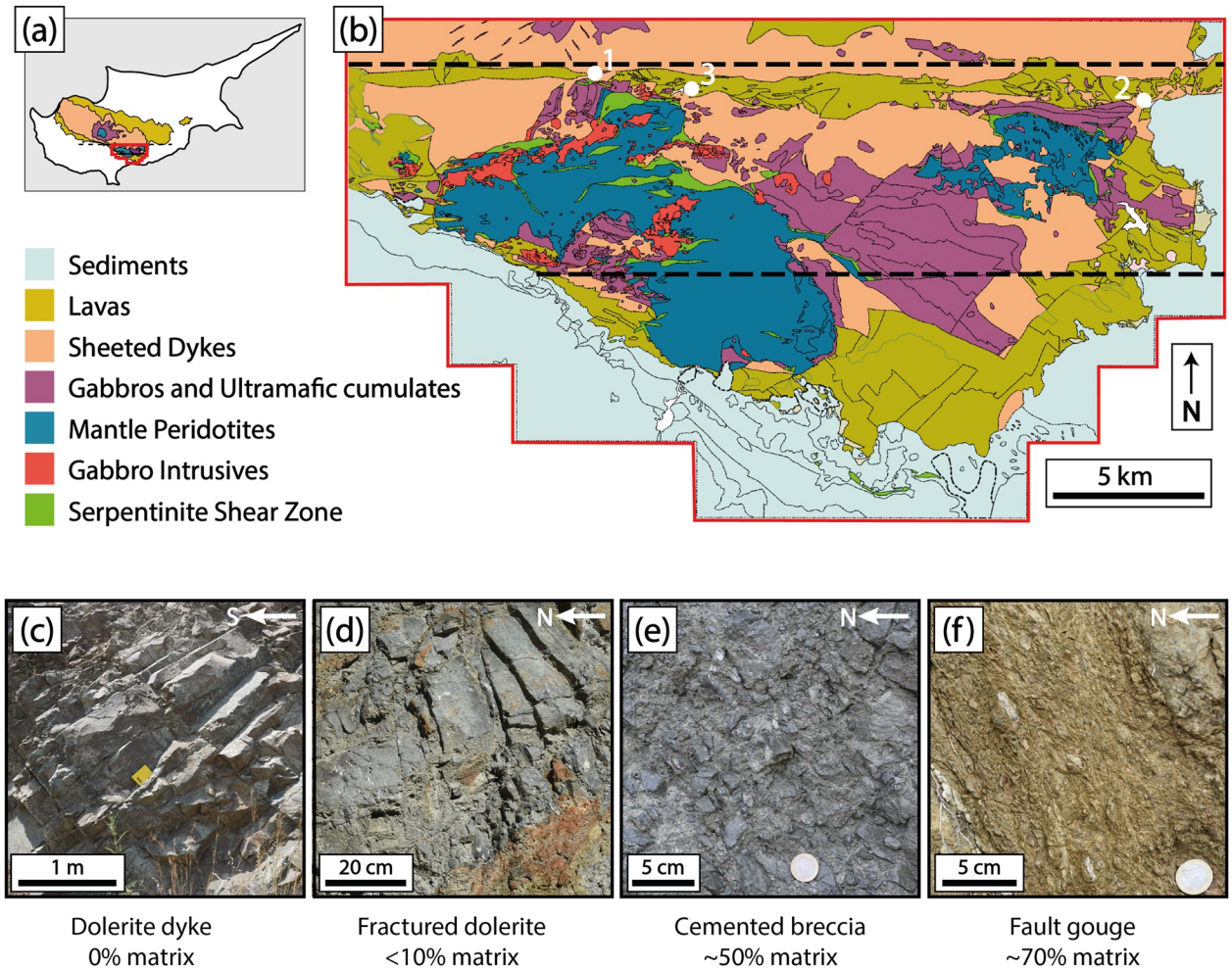

Figure 1. (a) Geological map of the Troodos ophiolite, Cyprus, and location of the Southern Troodos Transform Fault Zone (STTFZ) (red box). (b) Geological map of the STTFZ after Gass et al. (1994) showing sample locations for (1) cemented breccia, (2) matrix-rich breccia, and (3) fault gouge. (c)–(f) Field photographs illustrating the inferred progressive deformation of the STTFZ mafic crust.

velocity (V). During rapid changes in sample velocity, e.g., sample fracture or stick-slip events, these two velocities can deviate.

At the start of the experiment, we applied an initial constant displacement rate of 10 μm/s until a steady-state shear strength, τ, was reached, typically after ~5–6-mm displacement (Figure 2b). In some instances (e.g., dolerite and cemented breccia minicores; Figure S2), steady-state was not reached within 6 mm, in which case we measured τ at 6 mm to allow for comparison between experiments. We continually measured τ throughout the experiments and use this to calculate residual sliding friction coefficient, μ, as $\mu = \tau/\sigma_n'$, where σ_n' is the effective normal stress (σ_n—pore fluid pressure). This calculation of μ assumes that the samples are cohesionless; however, for some materials, such as those containing clay minerals, cohesion may not necessarily be negligible even during sliding (Ikari & Kopf, 2011); therefore, we report μ in this study as an "apparent" friction coefficient, which facilitates comparison with previous work.

Once steady-state shear strength (or 6-mm displacement) was reached, we began the velocity-step test (VST) experiment. We applied threefold increases in V_{lp} within the range of 0.1–30 μm/s (Figure 3a). For each velocity step, we measured the velocity-dependence of friction as the rate-and-state friction parameter $a–b$. $a–b$ is defined as $\Delta\mu_{ss}/\Delta\ln V$, where $\Delta\mu_{ss}$ is the change in steady-state friction after the change in sample velocity (e.g., Dieterich, 1979, 1981; Marone, 1998). The parameter $a–b$ is important in predicting fault slip behavior. Values of $a–b > 0$ indicate velocity-strengthening behavior and are associated with stable fault creep, whilst $a–b < 0$

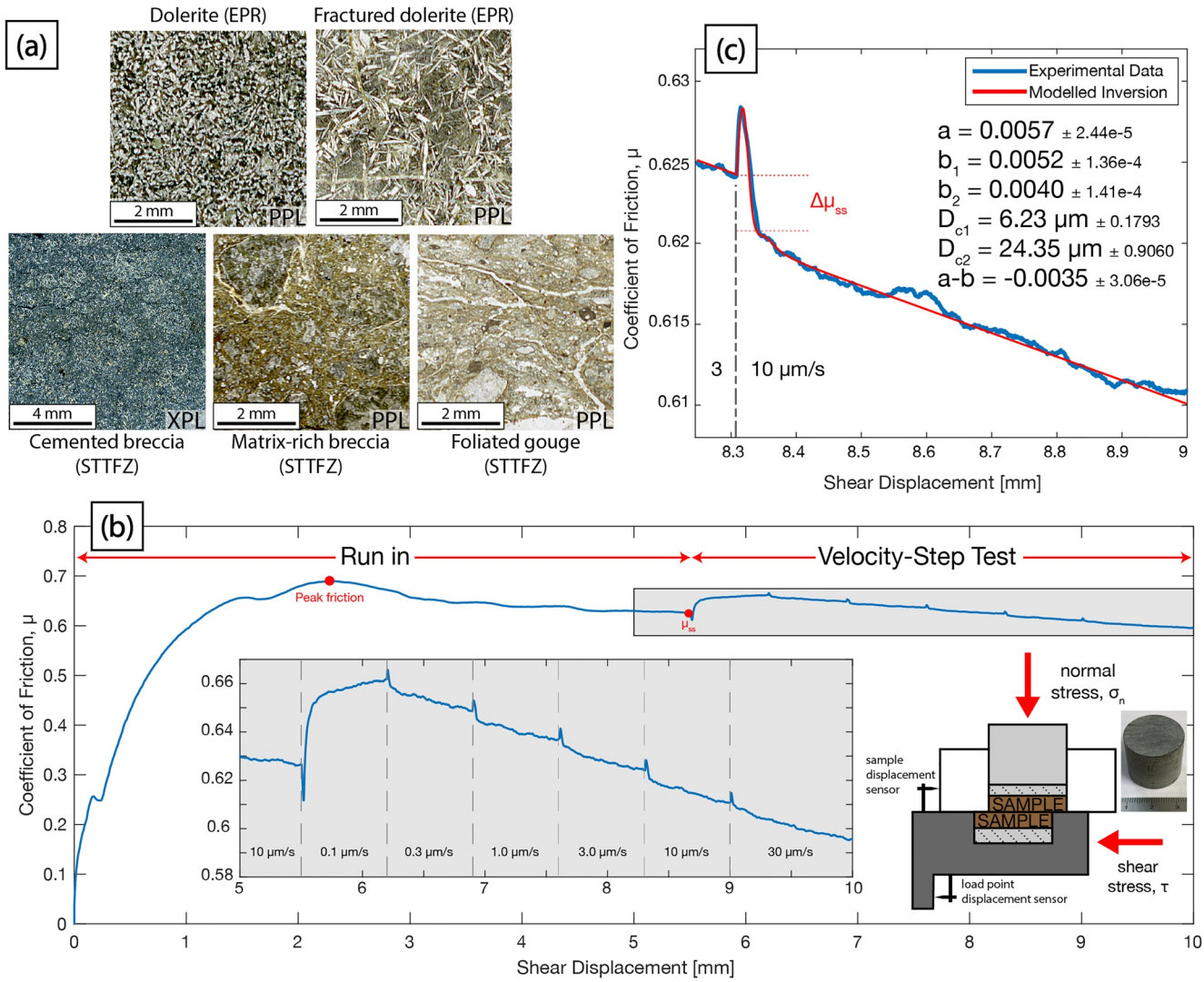

Figure 2. (a) Thin section scans of the starting materials for this study. (b) Example of a friction-displacement curve for (powdered) cemented breccia exhibiting velocity-weakening behavior ($a–b < 0$). Right inset shows a schematic representation of the laboratory setup. Larger inset shows a close-up of the velocity-step test. (c) Individual velocity step (3–10 µm/s from (b)), overlain with an inverse model (modeled using *RSFit3000*) from which rate-and-state friction parameters (as defined by Skarbek & Savage 2019) are obtained.

indicates velocity-weakening behavior (i.e., the strength of the rock decreases with increasing slip velocity), characteristic of unstable fault slip, and required for earthquake nucleation (Dieterich, 1979, 1981; Marone, 1998; Scholz, 1998). The frictional response to a velocity up-step can be described by the aging law, which explicitly considers that friction can evolve as a function of time and not necessarily slip (Dieterich & Kilgore, 1994). We use this law because it better describes natural phenomena (Kanu & Johnson, 2011; Rubin, 2008), but note that the slip law (Ruina, 1983) also fits our data well. For each velocity step, $a–b$ was calculated using inverse modeling techniques in *RSFit3000* (Skarbek & Savage, 2019) that yield the individual constitutive parameters a and b, where $b = b_1 + b_2$; however, in cases where the friction response to the velocity change is well described by a single-state variable, $b_2 = 0$.

Following the experiments, samples were dried, set in epoxy resin and cut parallel to the shear direction and perpendicular to the slip surface to analyze the slip surface in cross-section view. Backscattered scanning electron images were acquired using a Zeiss Sigma HD Field Emission Gun scanning electron microscope, operated in a high vacuum mode with an accelerating voltage of 20 kV and 60 µm aperture in the School of Earth and Environmental Sciences at Cardiff University.

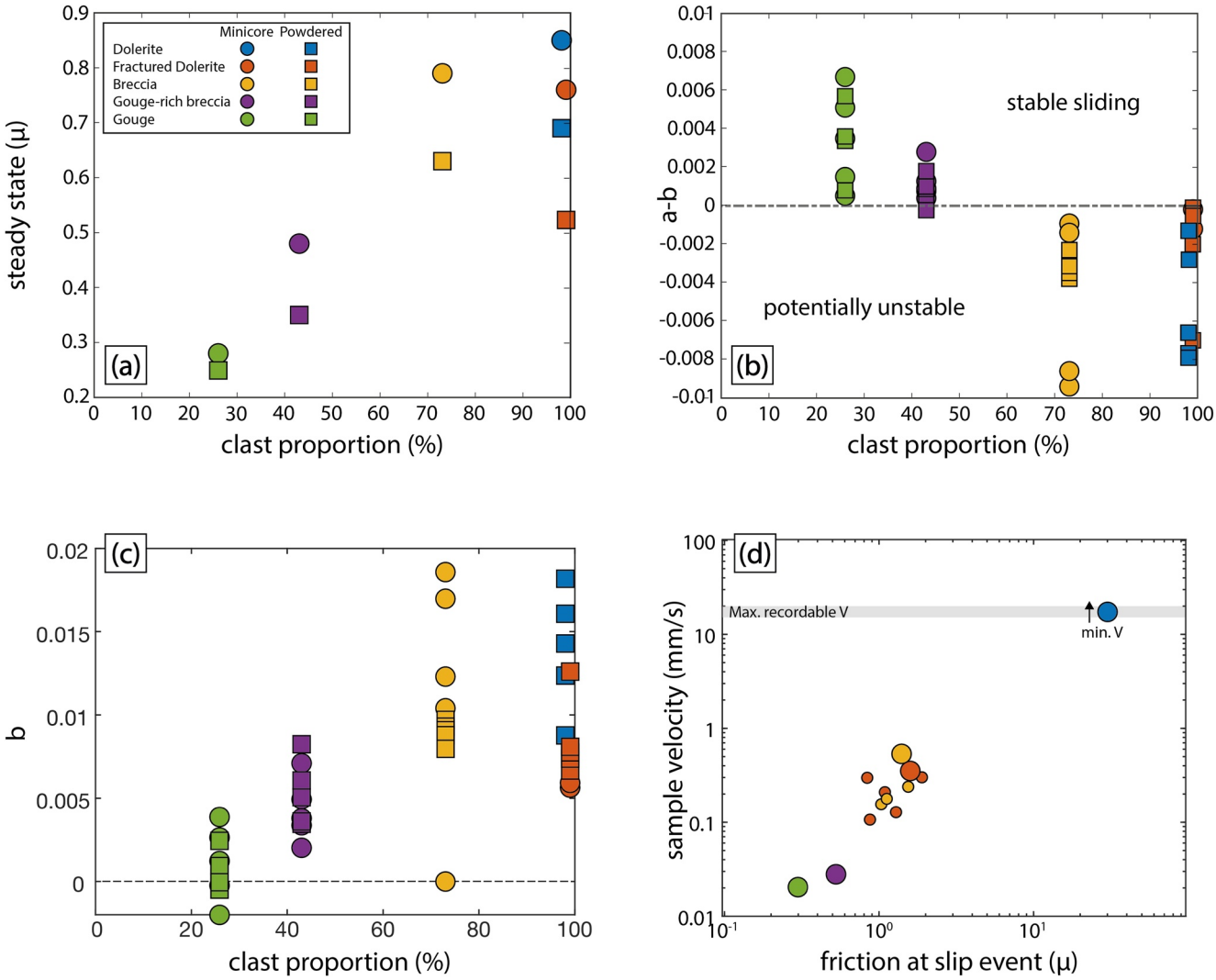

Figure 3. (a) Steady-state friction, (b) *a–b*, and (c) *b* as a function of clast proportion. (d) Peak sample velocity during failure of intact samples versus friction. Larger symbols represent the initial fracture for each experiment, smaller symbols represent subsequent breaks. Intact dolerite was broken under 1 MPa σ_n, all other samples under 10 MPa.

Mineralogy of each sample was determined using a combination of optical microscopy and X-ray diffraction (XRD) analysis (Figure S1 in Supporting Information S1). XRD analysis was carried out on powdered samples using a Philips PW1710 Automated Powder Diffractometer using Cu-Kα radiation at 35 kV and 40 mA. Analysis was carried out at a scan rate of 0.02°2θ/s between 2 and 70°2θ.

3. Results

3.1. Frictional Strength of Fault Rocks

Steady-state friction for minicores decreases linearly ($R = 0.94$) with decreasing clast proportion from $\mu = 0.85$ in EPR dolerite to $\mu = 0.28$ in the chlorite-rich fault gouge (Figures 3a and S2 in Supporting Information S1). For powdered samples, the correlation is also linear ($R = 0.87$), but the steady-state friction is systematically lower, with $\mu = 0.69$ in EPR dolerite, decreasing to 0.25 in the chlorite-rich gouge (Figures 3a and S2 in Supporting Information S1).

3.2. Velocity-Dependence of Friction

For the EPR dolerites and STTFZ cemented breccia, velocity-weakening frictional behavior is observed in both intact and powdered samples (Figure 3b). Only two $a–b$ values were determined for the fractured dolerite minicore, and none for the dolerite minicore, because of irregular fluctuations in the data that likely arise from roughness of the induced fracture surfaces. Velocity-strengthening frictional behavior is observed in both intact and powdered STTFZ fault gouge. The matrix-rich breccia sample is dominantly velocity-strengthening, with positive $a–b$ values for the minicore, and $a–b$ from −0.0002 to 0.0018 for the powdered sample (Figure 3b). We observe no dependence of $a–b$ on sliding velocity (Figure S3 in Supporting Information S1). The transition from velocity-weakening to velocity-strengthening behavior correlates with a decrease in b (Figure 3c) whereas a varies less (Figure S4 in Supporting Information S1).

Overall, $a–b$ increases with decreasing clast proportion, with the dolerite having the lowest $a–b$ and fault gouge has the highest. $a–b$ also correlates with μ, with a crossover in behavior from velocity-strengthening to velocity-weakening at $\mu \approx 0.5$ (Figure S5 in Supporting Information S1), consistent with previous experimental work (Ikari, Marone, & Saffer, 2011).

3.3. Initial Rock Failure

A range of peak sliding velocities occurred during the initial failure of the minicore samples. V of the fault gouge and matrix-rich breccia largely reflected the applied slip rate, reaching maximum slip speeds of ∼0.02–0.03 mm/s. However, the cemented breccia and both dolerite samples showed distinct frictional slip events where V exceeded the applied rate. The cemented breccia and fractured dolerite exhibited peak sliding velocities reaching 0.55 and 0.36 mm/s, respectively (Figure 3d). The dolerite minicore slipped audibly at a velocity of 18.65 mm/s immediately following peak friction (Figure 3d). Sampling rate limits the maximum measurable V in the direct-shear device to ∼15–20 mm/s, suggesting that our recorded value of 18.65 mm/s is a minimum value. Slip velocities of mm/s are rare in direct-shear experiments, and a $V > 1$ mm/s falls within the range of slip speeds that can generate seismic waves (e.g., Rowe & Griffith, 2015).

3.4. Microstructural Observations

Cross-sectional backscattered electron images of the sheared samples show that brittle fracture and grain-size reduction are common processes over an irregular zone of deformation up to ∼4-mm thick within the dolerite and breccia minicores (Figures 4a and 4c), and up to ∼0.5 mm on either side of the shear zone within the dolerite and breccia powders (Figures 4b and 4d). In the dolerite minicore, fragments up to several millimeters in length are surrounded by much finer clasts down to ∼1 μm (Figure S6a in Supporting Information S1). The cemented breccia minicore also shows fine clasts sizes down to ∼1 μm that surround fragments up to ∼2 mm in the shear zone (Figures 4c and S6c in Supporting Information S1). The fragment size in the experimentally deformed cemented breccia minicore is, in part, controlled by the size of the pre-existing dolerite clasts. Riedel (R) shears formed during experimental deformation of the EPR dolerites and the STTFZ cemented breccia (Figures 4a and 4c).

The matrix-rich breccia shows a weakly developed, discontinuous foliation accompanied by grain-size reduction over a zone ∼3 mm thick in the minicore and <1 mm in the powdered sample (Figures 4e, 4f and S6e in Supporting Information S1). The fault gouge sample shows a well-developed chlorite-defined foliation (Figures 4 and S7 in Supporting Information S1), bending toward parallelism with a narrower, ∼1–3 mm wide, shear zone, defined by interconnected and aligned chlorite grains in both the minicore and powdered samples (Figures 4g–4i and S6f, S6g in Supporting Information S1).

4. Discussion

4.1. Frictional Strength of Intact and Faulted Mafic Crust

Our results show a clear correlation between frictional strength and clast proportion (Figure 3a). The high frictional strength obtained for the EPR dolerites is related to a load-bearing framework of minerals (albite, actinolite, relict pyroxene) developed at greenschist facies hydrothermal conditions. These minerals are relatively strong in laboratory experiments performed at greenschist facies pressures and temperatures ($\mu > 0.7$; He et al., 2013).

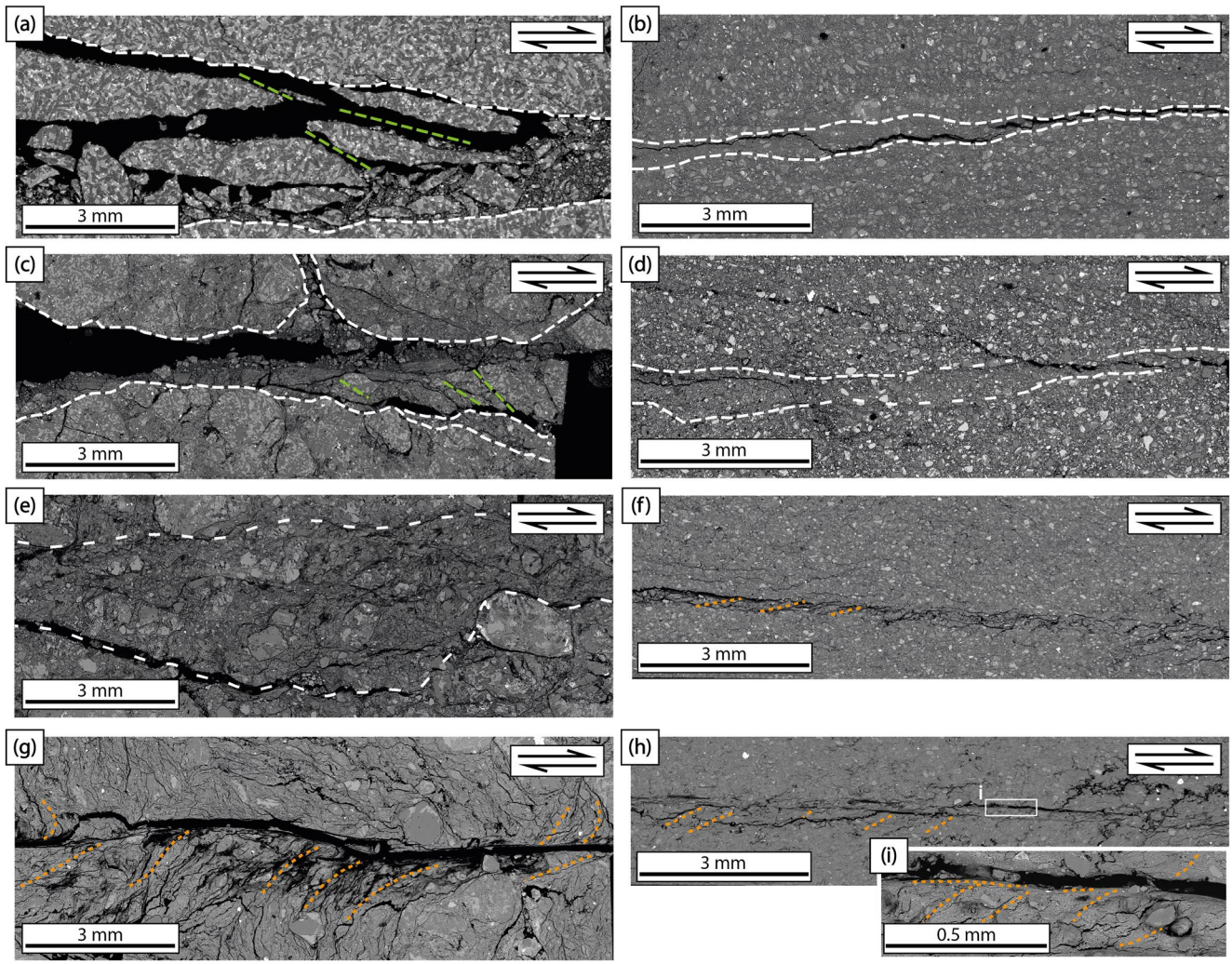

Figure 4. Backscattered scanning electron images of sheared: (a) dolerite minicore; (b) powdered dolerite; (c) cemented breccia minicore; (d) powdered cemented breccia; (e) matrix-rich breccia minicore; (f) matrix-rich breccia powder; (g) gouge minicore; and (h)–(i) powdered gouge. Dashed white lines show approximate boundaries of shear deformation. Fractures with orientations representing Riedel (R) shears are shown in green. Dashed orange lines highlight foliations.

The STTFZ cemented breccia is cemented with an albite-actinolite mineral assemblage (±minor quartz), indicating it also experienced greenschist facies hydrothermal conditions. Because of this cement, the breccia is relatively strong despite being more faulted and having a lower clast proportion than the EPR dolerites. In contrast, the matrix-rich breccia and fault gouge samples show steady-state frictional strengths that are much lower. In the dolerites, the chlorite proportion is small relative to matrix-rich breccia and fault gouge (Figures 4 and S7 in Supporting Information S1). Chlorite is known to be weak ($\mu \sim 0.3$) under almost all laboratory conditions from room temperature and 10 MPa pressure (Fagereng & Ikari, 2020), up to 400 MPa and 600 °C (Okamoto et al., 2019), and therefore, the weakness of the matrix-rich breccia and fault gouge can be attributed to an increase in chlorite content.

Interconnectivity of the weak phase can lead to more weakening than expected for a given volume fraction (Escartín et al., 2001; Handy, 1990), but our experiments show an approximately linear strength decrease with increasing matrix fraction (Figure 3a). A foliation was present prior to laboratory deformation of the fault gouge minicore and developed during the experiments on the powdered fault gouge sample (Figures 4h and 4i). This agrees with field observations that a foliation develops in the most mature, highly strained faults, and suggests gouge deformation occurs by sliding along chlorite basal planes that define the foliation. Phyllosilicate alignment can result in fault weakening (Collettini et al., 2009; Holdsworth et al., 2011; Ikari, Niemeijer, & Marone, 2011; Schleicher et al., 2010) and allows shear to localize onto foliation planes (Haines et al., 2013). The less

well-developed and less interconnected foliation in the matrix-rich breccia may therefore explain why it remains stronger than the foliated fault gouge where the chlorite is interconnected.

The strength difference between the minicore and powdered samples of the matrix-rich breccia and fault gouge is smaller than for the EPR dolerites and the cemented breccia (Figure 3a). The difference in strength between powders and minicores can be attributed to minicore cohesion (defined as the shear strength at $\sigma_n = 0$) being greater for the cemented rocks compared to more damaged ones. Assuming μ is equal for minicores and powders, cohesion is ~35 and ~14 MPa for the EPR dolerite samples, ~9 MPa for the cemented breccia sample, and ~1.6 and ~0.6 MPa for matrix-rich breccia and gouge samples, respectively.

4.2. Frictional Stability of Dolerite and Dolerite-Derived Fault Rocks

EPR dolerite and STTFZ cemented breccia are velocity-weakening (Figure 3b), consistent with the brittle fractures that developed (Figures 4a–4d). In contrast, the chlorite-rich STTFZ matrix-rich breccia and fault gouge are velocity-strengthening (Figure 3b), behavior consistent with other studies of foliated, chlorite-rich fault gouges (e.g., Imber et al., 1997; Schleicher et al., 2012; Smith & Faulkner, 2010). The tendency for frictional weakness to be associated with velocity-strengthening behavior (Figures 3a, 3b and S5 in Supporting Information S1) is consistent with previous work on a wide range of natural and analogue fault gouges (e.g., An et al., 2021; Ikari et al., 2016; Shimamoto & Logan, 1981; Tesei et al., 2012).

The change in frictional stability, $a–b$, with decreasing clast proportion is largely controlled by a decrease in the friction rate parameter b (Figure 3c). b describes the velocity-dependent loss in strength caused by changes in contact area (the "evolution effect"; Dieterich & Kilgore, 1994). Since our matrix-rich breccia and foliated fault gouge comprises well-aligned platy chlorite grains (Figures 4g–4i), the grain contact area may be at a maximum, explaining low values of b (Ikari et al., 2016; Saffer & Marone, 2003).

In the STTFZ samples, the change in slip behavior from velocity-weakening to velocity-strengthening is consistent with an increase in fault zone damage (decreased clast proportion) and associated alteration (increase in chlorite content and its interconnectivity), which may be a general feature of oceanic transforms. Brittle fractures, as observed in the dolerites and cemented breccia (Figures 4a–4d), provide a mechanism for increasing the permeability of the faults. This increased permeability can enhance fluid flow and alteration to chlorite, as suggested for rupture barrier regions along active oceanic transforms (e.g., Froment et al., 2014; Roland et al., 2010, 2012).

4.3. Slip Behavior of Oceanic Transform Faults

The microstructures created during the experiments (Figure 4) are comparable to those in the natural fault rocks. Although laboratory-derived frictional properties may (e.g., Blanpied et al., 1995) or may not (e.g., Moore & Lockner, 2008) change with P-T conditions, we infer that similar experimental and natural microstructures indicate that our results are broadly applicable within the upper oceanic crust. Furthermore, the relative weakening that occurs with increased chlorite content likely holds throughout the oceanic crust, as other experiments have shown chlorite to remain weak ($\mu \leq 0.4$) up to 600 °C (Okamoto et al., 2019).

Applied to oceanic transforms, our experimental observations are consistent with geophysical inferences that (a) along-strike changes in seismic behavior are controlled variable fault zone damage and alteration (Froment et al., 2014; Roland et al., 2010, 2012), and (b) faults within the transform domain are frictionally weaker than the surrounding crust (Behn et al., 2002; Beutel & Okal, 2003; Homberg et al., 2010). Crustal transform faults that contain matrix-rich or gouge-rich material with interconnected phyllosilicates are likely to be weak and have low seismic coupling, as has been inferred for some segments of active oceanic transforms that have low seismic velocities (e.g., Froment et al., 2014; McGuire et al., 2012; Roland et al., 2012), whereas regions of the crust that have not experienced much damage or alteration, or are cemented, are strong and are capable of hosting earthquake slip. This is supported by a correlation between frictional weakness and frictional stability (Figures 3a and 3b), and audible slip at relatively fast rates recorded during initial the fracturing (Figure 3d; >1 mm/s) of dolerite and cemented breccia samples, whereas such fast rates were not recorded when shearing samples with a small dolerite clast proportion. These results suggest that the formation of interconnected chlorite may play an important role on the rheology of oceanic transforms. Comparably, at mantle depths, strength contrasts between

faults and wall rocks may also be related to hydration and alteration to fine-grained mylonites (Kohli et al., 2021) and foliated serpentinite (Cox et al., 2021).

The progressive transition in frictional strength and behavior observed here could be taken to suggest that oceanic transforms should become more aseismic with age. However, no such age-seismicity relationships are observed along active oceanic transforms. Since deformation in active oceanic transforms occurs along pre-existing fractures such as dyke margins and cooling joints (e.g., Bergerat et al., 2000; Homberg et al., 2010; MacLeod & Murton, 1993), which occur in a range of orientations, there are abundant new surfaces for fault strands to form along and continue to supply new intact material. Geometrical complexities (e.g., Macdonald et al., 1986; Pockalny et al., 1988; Searle, 1981) and spatial variation in damage and alteration can therefore result in a heterogeneous seismic behavior. New intact dolerite, here found to be strong and velocity-weakening, can be continually faulted leading to the local nucleation of seismicity as intact dolerite rocks fracture (Figure 3d), even if mature fault zones have developed elsewhere.

5. Conclusions

We conducted direct-shear friction experiments on intact and powdered samples of dolerite from the East Pacific Rise (Hess Deep) and a series of mafic fault rocks from the exhumed Southern Troodos Transform Fault Zone, Cyprus. With decreasing dolerite clast proportion (hence increasing volume fraction of phyllosilicate-rich matrix), frictional strength decreases from $\mu = 0.85$ to 0.28 in minicore and from $\mu = 0.69$ to 0.25 in powdered samples, and frictional stability changes from velocity-weakening to velocity-strengthening. We deduce that, in modern oceanic transforms, continuing deformation along faults leads to progressive changes in composition, from frictionally strong minerals in dolerite to increasing proportion and interconnectivity of frictionally weak phyllosilicates (chlorite) in matrix-rich and gouge-rich fault rocks. This gradual change occurs over multiple earthquakes cycles and is assisted by fluid flow to facilitate phyllosilicate growth as transform faulting proceeds. Our direct observation that frictional stability changes with fault rock type agrees with inferences from geophysical observations along active oceanic transforms, which suggest poorly-coupled fault segments are characterized by increased damage and alteration.

Conflict of Interest

The authors declare no conflicts of interest relevant to this study.

Data Availability Statement

Velocity-dependent friction parameters can be accessed at https://doi.org/10.5281/zenodo.5708108.

Acknowledgments
Thanks to support from Director and staff of Cyprus Geological Survey Department. We thank Duncan Muir for assistance with scanning electron microscopy and Tony Oldroyd for sample preparation. SC is supported by a NERC GW4+ Doctoral Training Partnership studentship from the Natural Environment Research Council (NE/L002434/1), and by the University of Bremen and Cardiff University via the Bremen-Cardiff Alliance Fund. AF is supported by the European Research Council (ERC) Horizon 2020 Program (grant agreement 715836). We thank Keishi Okazaki and Margaret Boettcher for their constructive reviews that significantly improved this manuscript.

References

Abercrombie, R. E., & Ekström, G. (2001). Earthquake slip on oceanic transform faults. *Nature*, *410*, 74–77. https://doi.org/10.1038/35065064

An, M., Zhang, F., Min, K. B., Elsworth, D., Marone, C., & He, C. (2021). The potential for low-grade metamorphism to facilitate fault instability in a geothermal reservoir. *Geophysical Research Letters*, *48*, e2021GL093552. https://doi.org/10.1029/2021GL093552

Behn, M. D., Boettcher, M. S., & Hirth, G. (2007). Thermal structure of oceanic transform faults. *Geology*, *35*, 307–310. https://doi.org/10.1130/g23112a.1

Behn, M. D., Lin, J., & Zuber, M. T. (2002). Evidence for weak oceanic transform faults. *Geophysical Research Letters*, *29*(24), 2207. https://doi.org/10.1029/2002GL015612

Bergerat, F., Angelier, J., & Homberg, C. (2000). Tectonic analysis of the Husavik-Flatey Fault (northern Iceland) and mechanisms of an oceanic transform zone, the Tjörnes Fracture Zone. *Tectonics*, *19*, 1161–1177. https://doi.org/10.1029/2000TC900022

Beutel, E. K., & Okal, E. A. (2003). Strength asperities along oceanic transform faults: A model for the origin of extensional earthquakes on the Eltanin transform system. *Earth and Planetary Science Letters*, *216*, 27–41. https://doi.org/10.1016/s0012-821x(03)00484-9

Bird, P., Kagan, Y. Y., & Jackson, D. D. (2002). Plate tectonics and earthquake potential of spreading ridges and oceanic transform faults. In S. Stein & J. T. Freymueller (Eds.), *Plate boundary zones, Geodynamics Series* (Vol. 30, pp. 203–218). American Geophysical Union.

Blanpied, M. L., Lockner, D. A., & Byerlee, J. D. (1995). Frictional slip of granite at hydrothermal conditions. *Journal of Geophysical Research*, *100*, 13045–13064. https://doi.org/10.1029/95JB00862

Boettcher, M. S., & Jordan, T. H. (2004). Earthquake scaling relations for mid-ocean ridge transform faults. *Journal of Geophysical Research*, *109*, B12302. https://doi.org/10.1029/2004JB003110

Collettini, C., Niemeijer, A., Viti, C., & Marone, C. (2009). Fault zone fabric and fault weakness. *Nature*, *462*, 907–910. https://doi.org/10.1038/nature08585

Cox, S., Fagereng, Å., & MacLeod, C. J. (2021). Shear zone development in serpentinized mantle: Implications for the strength of oceanic transform faults. *Journal of Geophysical Research: Solid Earth*, *126*, e2020JB020763. https://doi.org/10.1029/2020JB020763

Cox, S. J. D. (1990). Velocity-dependent friction in a large direct shear experiment on gabbro. *Geological Society London, Special Publications*, *54*, 63–70. https://doi.org/10.1144/gsl.sp.1990.054.01.07

Dieterich, J. H. (1979). Modelling of rock friction: 1. Experimental results and constitutive equations. *Journal of Geophysical Research*, *84*, 2161–2168. https://doi.org/10.1029/JB084iB05p02161

Dieterich, J. H. (1981). Constitutive properties of faults with simulated gouge. In N. Carter, M. Friedman, J. Logan, & D. Stearns (Eds.), *Mechanical behaviour of crustal rocks* (pp. 103–120).

Dieterich, J. H., & Kilgore, B. D. (1994). Direct observation of frictional contacts: New insights for state-dependent properties. *Pure and Applied Geophysics*, *143*, 283–302. https://doi.org/10.1007/bf00874332

Escartín, J., Hirth, G., & Evans, B. (2001). Strength of slightly serpentinized peridotites: Implications for the tectonics of oceanic lithosphere. *Geology*, *29*, 1023–1026.

Escartín, J., Mével, C., MacLeod, C. J., & McCaig, A. M. (2003). Constraints on deformation conditions and the origin of oceanic detachments: The Mid-Atlantic Ridge core complex at 15°45′N. *Geochemistry, Geophysics, Geosystems*, *4*(8), 1067. https://doi.org/10.1029/2002GC000472

Fagereng, A., & Ikari, M. J. (2020). Low-temperature frictional characteristics of chlorite-epidote-amphibole assemblages: Implications for strength and seismic style of retrograde fault zones. *Journal of Geophysical Research: Solid Earth*, *125*, e2020JB019487. https://doi.org/10.1029/2020JB019487

Froment, B., McGuire, J. J., van der Hilst, R. D., Gouédard, P., Roland, E. C., Zhang, H., & Collins, J. A. (2014). Imaging along-strike variations in mechanical properties of the Gofar transform fault, East Pacific Rise. *Journal of Geophysical Research: Solid Earth*, *119*, 7175–7194. https://doi.org/10.1002/2014JB011270

Gass, I. G., MacLeod, C. J., Murton, B. J., Panayiotou, A., Simonian, K. O., & Xenophontos, C. (1994). *The Geology of the Southern Troodos Transform Fault Zone, Cyprus* (Vol. 9). Geological Survey Department Memoir.

Haines, S. H., Kaproth, B., Marone, C., Saffer, D., & van der Pluijm, B. (2013). Shear zones in clay-rich fault gouge: A laboratory study of fabric development and evolution. *Journal of Structural Geology*, *51*, 206–225. https://doi.org/10.1016/j.jsg.2013.01.002

Handy, M. R. (1990). The solid-state flow of polymineralic rocks. *Journal of Geophysical Research*, *95*, 8647–8661. https://doi.org/10.1029/JB095iB06p08647

He, C., Luo, L., Hao, Q.-M., & Zhou, Y. (2013). Velocity-weakening behaviour of plagioclase and pyroxene gouges and stabilizing effect of small amounts of quartz under hydrothermal conditions. *Journal of Geophysical Research: Solid Earth*, *118*, 3408–3430. https://doi.org/10.1002/jgrb.50280

He, C., Wang, Z., & Yao, W. (2007). Frictional sliding of gabbro gouge under hydrothermal conditions. *Tectonophysics*, *445*, 353–362. https://doi.org/10.1016/j.tecto.2007.09.008

Hilley, G. E., Sare, R. M., Aron, F., Baden, C. W., Caress, D. W., Castillo, C. M., et al. (2020). Coexisting seismic behaviour of transform faults revealed by high-resolution bathymetry. *Geology*, *48*, 379–384. https://doi.org/10.1130/g46663.1

Holdsworth, R. E., van Diggelen, E. W. E., Spiers, C. J., de Bresser, J. H. P., Walker, R. J., & Bowen, L. (2011). Fault rocks from the SAFOD core samples: Implications for weakening at shallow depths along the San Andreas Fault, California. *Journal of Structural Geology*, *33*, 132–144. https://doi.org/10.1016/j.jsg.2010.11.010

Homberg, C., Bergerat, F., Angelier, J., & Garcia, S. (2010). Fault interaction and stresses along broad oceanic transform zone: Tjörnes Fracture Zone, north Iceland. *Tectonics*, *29*, TC1002. https://doi.org/10.1029/2008TC002415

Ikari, M. J., Carpenter, B. M., & Marone, C. (2016). A microphysical interpretation of rate- and state-dependent friction for fault gouge. *Geochemistry, Geophysics, Geosystems*, *17*, 1660–1677. https://doi.org/10.1002/2016GC006286

Ikari, M. J., Kameda, J., Saffer, D. M., & Kopf, A. J. (2015). Strength characteristics of Japan Trench borehole samples in the high-slip region of the 2011 Tohoku-Oki earthquake. *Earth and Planetary Science Letters*, *412*, 35–41. https://doi.org/10.1016/j.epsl.2014.12.014

Ikari, M. J., & Kopf, A. J. (2011). Cohesive strength of clay-rich sediment. *Geophysical Research Letters*, *38*, L16309. https://doi.org/10.1029/2011GL047918

Ikari, M. J., Marone, C., & Saffer, D. M. (2011). On the relation between fault strength and frictional stability. *Geology*, *39*, 83–86. https://doi.org/10.1130/g31416.1

Ikari, M. J., Niemeijer, A. R., & Marone, C. (2011). The role of fault zone fabric and lithification state on frictional strength, constitutive behaviour, and deformation microstructure. *Journal of Geophysical Research*, *116*, B08404. https://doi.org/10.1029/2011JB008264

Imber, J., Holdsworth, R. E., Butler, C. A., & Lloyd, G. E. (1997). Fault zone weakening processes along the reactivated outer Hebrides fault zone, Scotland. *Journal of the Geological Society of London*, *154*, 105–109. https://doi.org/10.1144/gsjgs.154.1.0105

Kanu, C., & Johnson, K. (2011). Arrest and recovery of frictional creep on the southern Hayward fault triggered by the 1989 Loma Prieta, California, earthquake and implications for future earthquakes. *Journal of Geophysical Research*, *116*, B04403. https://doi.org/10.1029/2010JB007927

Kohli, A., Wolfson-Schwehr, M., Prigent, C., & Warren, J. M. (2021). Oceanic transform fault seismicity and slip mode influenced by seawater infiltration. *Nature Geoscience*, *14*, 606–611. https://doi.org/10.1038/s41561-021-00778-1

Macdonald, K. C., Castillo, D. A., Miller, S. P., Fox, P. J., Kastens, K. A., & Bonatti, E. (1986). Deep-tow studies of the Vema Fracture Zone 1. Tectonics of a major slow slipping transform fault and its intersection with the Mid-Atlantic Ridge. *Journal of Geophysical Research*, *91*, 3334–3354. https://doi.org/10.1029/JB091iB03p03334

MacLeod, C. J., Escartín, J., Banerji, D., Banks, G. J., Irving, D. H. B., Lilly, R. M., et al. (2002). Direct geological evidence for oceanic detachment faulting: The mid Atlantic ridge, 14°45′N. *Geology*, *30*, 879–882. https://doi.org/10.1130/0091-7613(2002)030<0879:dgefod>2.0.co;2

MacLeod, C. J., & Murton, B. J. (1993). Structure and tectonic evolution of the southern Troodos transform fault zone, Cyprus. *Geological Society, London, Special Publications*, *76*, 141–176. https://doi.org/10.1144/gsl.sp.1993.076.01.07

MacLeod, C. J., Teagle, D. A. H., Gillis, K. M., Cazenave, P. W., Hansen, H. E., Howard, K. A., et al. (2008). *Accretion of the lower oceanic crust at fast-spreading ridges: A rock drill and near-bottom seafloor survey in support of IODP drilling in Hess Deep* (Technical report). Cardiff University.

Marone, C. (1998). Laboratory-derived frictional laws and their application to seismic faulting. *Annual Review of Earth and Planetary Sciences*, *26*, 642–696. https://doi.org/10.1146/annurev.earth.26.1.643

McGuire, J. J. (2008). Seismic cycles and earthquake predictability on East Pacific Rise transform faults. *Bulletin of the Seismological Society of America*, *98*, 1067–1084. https://doi.org/10.1785/0120070154

McGuire, J. J., Boettcher, M. S., & Jordan, T. H. (2005). Foreshock sequences and short-term earthquake predictability on East Pacific Rise transform faults. *Nature*, *434*(7032), 457–461. https://doi.org/10.1038/nature03377

McGuire, J. J., Collins, J. A., Gouédard, P., Roland, E., Lizarralde, D., Boettcher, M. S., et al. (2012). Variations in earthquake rupture properties along the Gofar transform fault, East Pacific Rise. *Nature Geoscience*, *5*, 336–341. https://doi.org/10.1038/ngeo1454

McGuire, J. J., Ihmle, P. F., & Jordan, T. H. (1996). Time-domain observations of a slow precursor to the 1994 Romanche transform earthquake. *Science*, *274*, 82–85. https://doi.org/10.1126/science.274.5284.82

Moore, D. E., & Lockner, D. A. (2008). Talc friction in the temperature range 25-400°C: Relevance for fault-zone weakening. *Tectonophysics*, *449*, 120–132. https://doi.org/10.1016/j.tecto.2007.11.039

Moore, D. E., Lockner, D. A., Shengli, M., Summers, R., & Byerlee, J. D. (1997). Strengths of serpentinite gouges at elevated temperatures. *Journal of Geophysical Research*, *102*, 14787–14801. https://doi.org/10.1029/97JB00995

Okamoto, A. S., Verberne, B. A., Niemeijer, A. R., Takahashi, M., Shimizu, I., Ueda, T., & Spiers, C. J. (2019). Frictional properties of simulated chlorite gouge at hydrothermal conditions: Implications for subduction megathrusts. *Journal of Geophysical Research: Solid Earth*, *124*, 4545–4565. https://doi.org/10.1029/2018JB017205

Phillips, N. J., Belzer, B., French, M. E., Rowe, C. D., & Ujiie, K. (2020). Frictional strengths of subduction thrust rocks in the region of shallow slow earthquakes. *Journal of Geophysical Research: Solid Earth*, *125*, e2019JB018888. https://doi.org/10.1029/2019JB018888

Pockalny, R. A., Detrick, R. S., & Fox, P. J. (1988). Morphology and tectonics of the Kane transform from Sea Beam bathymetry data. *Journal of Geophysical Research*, *93*, 3179–3193. https://doi.org/10.1029/JB093iB04p03179

Roland, E., Behn, M. D., & Hirth, G. (2010). Thermal-mechanical behaviour of oceanic transform faults: Implications for the spatial distribution of seismicity. *Geochemistry, Geophysics, Geosystems*, *11*, Q07001. https://doi.org/10.1029/2010GC003034

Roland, E., Lizarralde, D., McGuire, J. J., & Collins, J. A. (2012). Seismic velocity constraints on the material properties that control earthquake behaviour at the Quebrada-Discovery-Gofar transform faults, East Pacific Rise. *Journal of Geophysical Research*, *117*, B11102. https://doi.org/10.1029/2012JB009422

Rowe, C. D., & Griffith, W. A. (2015). Do faults preserve a record of seismic slip: A second opinion. *Journal of Structural Geology*, *78*, 1–26. https://doi.org/10.1016/j.jsg.2015.06.006

Rubin, A. M. (2008). Episodic slow slip events and rate-and-state friction. *Journal of Geophysical Research*, *113*, B11414. https://doi.org/10.1029/2008JB005642

Ruina, A. (1983). Slip instability and state variable friction laws. *Journal of Geophysical Research*, *88*, 10359–10370. https://doi.org/10.1029/JB088iB12p10359

Saffer, D. M., & Marone, C. (2003). Comparison of smectite- and illite-rich gouge frictional properties: Application to the up-dip limit of the seismogenic zone along subduction megathrusts. *Earth and Planetary Science Letters*, *215*, 219–235. https://doi.org/10.1016/s0012-821x(03)00424-2

Schleicher, A. M., van der Pluijm, B. A., & Warr, L. N. (2010). Nanocoatings of clay and creep of the San Andreas fault at Parkfield, California. *Geology*, *38*, 667–670. https://doi.org/10.1130/g31091.1

Schleicher, A. M., van der Pluijm, B. A., & Warr, L. N. (2012). Chlorite smectite clay minerals and fault behaviour: New evidence from the San Andreas fault observatory at depth (SAFOD) core. *Lithosphere*, *4*, 209–220. https://doi.org/10.1130/l158.1

Scholz, C. H. (1998). Earthquake and friction laws. *Nature*, *391*, 37–42. https://doi.org/10.1038/34097

Searle, R. (1981). The active part of Charlie-Gibbs fracture zone: A study using sonar and other geophysical techniques. *Journal of Geophysical Research*, *81*, 243–262. https://doi.org/10.1029/JB086iB01p00243

Shimamoto, T., & Logan, J. M. (1981). Effects of simulated clay gouges on the sliding behaviour of Tennessee Sandstone. *Tectonophysics*, *75*, 243–255. https://doi.org/10.1016/0040-1951(81)90276-6

Sibson, R. H. (1977). Fault rocks and fault mechanisms. *Journal of the Geological Society of London*, *133*, 191–213. https://doi.org/10.1144/gsjgs.133.3.0191

Skarbek, R. M., & Savage, H. M. (2019). RSFit3000: A MATLAB GUI-based program for determining rate and state frictional parameters from experimental data. *Geosphere*, *15*, 1665–1676. https://doi.org/10.1130/ges02122.1

Smith, S. A. F., & Faulkner, D. R. (2010). Laboratory measurements of the frictional properties of the Zuccale low-angle normal fault, Elba Island, Italy. *Journal of Geophysical Research*, *115*, B02407. https://doi.org/10.1029/2008JB006274

Sykes, L. R., & Ekström, G. (2012). Earthquakes along Eltanin transform system, SE Pacific Ocean: Fault segments characterized by strong and poor seismic coupling and implications for long-term earthquake prediction. *Geophysical Journal International*, *188*, 421–434.

Tesei, T., Collettini, C., Carpenter, B. M., Viti, C., & Marone, C. (2012). Frictional strength and healing behaviour of phyllosilicate-rich faults. *Journal of Geophysical Research*, *117*, B09402. https://doi.org/10.1029/2012JB009204

Wolfson-Schwehr, M., Boettcher, M. S., McGuire, J. J., & Collins, J. A. (2014). The relationship between seismicity and fault structure on the Discovery transform fault, East Pacific Rise. *Geochemistry, Geophysics, Geosystems*, *15*, 3698–3712. https://doi.org/10.1002/2014GC005445

Zhang, L., He, C., Liu, Y., & Lin, J. (2017). Frictional properties of the South China Sea oceanic basalt and implications for strength of the Manila subduction seismogenic zone. *Marine Geology*, *394*, 16–29. https://doi.org/10.1016/j.margeo.2017.05.006

Zoback, M. D. (1991). State of stress and crustal deformation along weak transform faults. *Philosophical Transactions: Physical Sciences and Engineering*, *337*, 141–150.